Applied Catalysis B: Environmental 90 (2009) 195–204

Contents lists available at ScienceDirect

Applied Catalysis B: Environmental

journal homepage: www.elsevier.com/locate/apcatb

Steam reforming of methanol over CeO_2- and ZrO_2-promoted Cu-ZnO catalysts supported on nanoparticle Al_2O_3

Samuel D. Jones, Helena E. Hagelin-Weaver *

Department of Chemical Engineering, University of Florida, Gainesville, FL 32611, United States

ARTICLE INFO

Article history:
Received 30 August 2008
Received in revised form 19 December 2008
Accepted 6 March 2009
Available online 19 March 2009

Keywords:
Methanol steam reforming
Copper catalyst
$Cu/ZnO/CeO_2/Al_2O_3$
$Cu/ZnO/ZrO_2/Al_2O_3$
Hydrogen production
Nanoparticle alumina
Nanoparticle zirconia
CO selectivity
TPR
XRD

ABSTRACT

Methanol steam reforming was studied over several ZrO_2- and CeO_2-promoted catalysts prepared by deposition of copper and zinc oxide precursors onto nanoparticle Al_2O_3 and ZrO_2 supports. The catalysts were characterized using temperature programmed reduction (TPR), Brunauer–Emmett–Teller (BET) surface area measurements, N_2O decomposition, and X-ray diffraction (XRD) and the results were compared to a commercially available $Cu/ZnO/Al_2O_3$ catalyst. It was found that the catalyst activities and CO selectivities are very dependent on both the catalyst preparation method and the ZrO_2 precursor. The best performing catalyst was prepared by co-impregnating Cu and ZnO precursors onto a physical mixture of nanoparticle ZrO_2 and nanoparticle Al_2O_3. This catalyst resulted in a highly active reforming catalyst which also suppressed CO production. The turnover frequencies of catalysts containing ZrO_2 nanoparticles were notably higher than those of similar catalysts which contained impregnated ZrO_2, and dramatically higher than the commercially available reference catalyst. This indicates that the presence of ZrO_2 nanoparticles promotes a highly active copper surface. Addition of high surface area alumina was necessary to assure a reasonable Cu surface area. However, the catalytic activities of the catalysts in this study did not correlate with Cu surface area, total surface area, or reduction temperature. It is therefore postulated that the presence of a monoclinic ZrO_2 phase, which is a result of using a monoclinic nanoparticle ZrO_2 precursor, promotes methanol reforming and also suppresses methanol decomposition, both of which are desired in methanol reforming catalysts.

1. Introduction

Increasing costs in petroleum production and environmental factors have driven research into alternatives to fossil fuel based energy sources over the last two decades. Hydrogen energy has long been a promising alternative to fossil fuel sources. Specifically, hydrogen produced via methanol reforming can be fed to a Proton Exchange Membrane Fuel Cell (PEMFC) to generate electricity. Although research into making the use of PEMFC units widespread is more recent, the first practical use of a PEMFC power source was aboard the Gemini space missions of the 1960s [1]. Unlike internal combustion engines, PEMFC units have no moving parts, do not produce sulfur or nitrous oxides, and as an electrochemical energy source, are not restricted by the thermodynamic limits of the Carnot efficiency [1]. The chemical reactions involved in methanol reforming are the steam reforming reaction (Eq. (1)), the water–gas shift (2), and the methanol decomposition reaction (3).

$$CH_3OH + H_2O \rightarrow 3H_2 + CO_2 \quad (1)$$

$$CO + H_2O \leftrightarrow CO_2 + H_2 \quad (2)$$

$$CH_3OH \rightarrow 2H_2 + CO \quad (3)$$

Formation of CO is to be avoided in methanol reforming to the greatest extent possible, since CO is a poison to the platinum cathode in the PEMFC assembly at concentrations as low as 10 ppm [1–3]. CO production is usually measured by the "CO selectivity", or the molar ratio of CO formed to the total CO plus CO_2 produced in the reaction, as defined in Eq. (4).

$$S = \frac{P_{CO}}{P_{CO} + P_{CO_2}} \times 100\% \quad (4)$$

In this equation P_{CO_x} are the molar concentrations or partial pressures of CO and CO_2 gas. There are two potential sources of CO in the reforming reaction network; the reverse water–gas shift and the direct methanol decomposition. Peppley et al., showed in their work that the CO levels in the reforming reactor effluent were higher than could be explained by the water–gas shift equilibrium, and therefore concluded that decomposition must be taken into account [4]. However, other studies using different catalysts have shown that the CO content is below what can be explained via the water–gas shift equilibrium [5], and that the CO production rate is

* Corresponding author. Tel.: +1 352 392 6585; fax: +1 352 392 9513.
E-mail address: hweaver@che.ufl.edu (H.E. Hagelin-Weaver).

0926-3373/$ – see front matter © 2009 Elsevier B.V. All rights reserved.
doi:10.1016/j.apcatb.2009.03.013

more consistent with CO being a secondary product, i.e. CO is formed exclusively through the reverse water–gas shift [2,6,7]. Evidently the pathways for CO production are highly sensitive to the catalysts in use.

Conventional $Cu/ZnO/Al_2O_3$ catalysts often consist of relatively large amounts of Cu and ZnO and a small amount of Al_2O_3 [8]. The ZnO is added to improve the Cu dispersion and the redox properties of the copper phases, while the alumina is added to increase the surface area and to reduce Cu sintering [9]. Only small amounts of Al_2O_3 can be used, since higher concentrations can have a negative effect on the catalytic activity [10,11]. Due to the negative effects of Al_2O_3 supports in methanol reforming catalysts, the trend in recent years is to add another component to the $Cu/ZnO/Al_2O_3$ catalysts or simply use supports other than alumina. Reducible metal oxides, such as ZrO_2 and CeO_2, appear to be attractive alternatives or additions to Al_2O_3 [2,6,12–23]. For example, ZrO_2 addition to Cu-based alumina-supported catalysts has been shown to increase methanol conversion and reduce CO yields [13–16]. The effects of ZrO_2 on Cu-based catalysts appear to be similar to the effects of ZnO in that ZrO_2 improves Cu dispersion and leads to more reducible catalysts [6,14–16]. However, it has been noted that the metal–support interactions in Cu/ZrO_2 are different than in the more conventional Cu/ZnO catalysts [24]. Some authors even describe a "synergy" between the Cu and ZrO_2 [6]. The higher activity of Cu-ZrO_2 catalysts has also been attributed to the stabilization of Cu_2O on the surface of the reduced catalysts or during the reaction [15,18,19]. It is believed that the formation of Cu_2O leads to both more active and more durable catalysts, since Cu_2O is less susceptible to sintering compared with Cu metal [18,19]. Cu^+ species have also been observed in CeO_2-containing Cu catalysts [17,25]. Addition of CeO_2 to Cu/Al_2O_3 catalysts has also been shown to increase methanol conversion, decrease CO selectivity and increase catalyst stability [26].

Numerous studies of ZrO_2- or CeO_2-promoted Cu-based methanol steam reforming catalysts are available in the literature [2,3,6,7,10,12–26]. However, comparing results between studies is challenging since the reaction evidently is very sensitive to the catalysts used and large differences in Cu loadings and catalyst compositions have been reported. For example, the copper concentrations on these types of catalysts have been varied from a few percent in some publications [12,17] up to 70% or above in others [6]. Some catalysts also contain ZnO and Al_2O_3 in addition to Cu and ZrO_2 [6,13,15,16]. Therefore, when comparing different methanol steam reforming catalysts it is important to include reference catalysts for comparisons.

Previous results from our group have shown that using nanoparticle alumina as the support for Cu-ZnO-based methanol steam reforming catalysts leads to catalysts with lower CO selectivity and similar conversions compared to commercially available catalysts. The objective in the present study is to investigate if the catalytic activity (methanol conversion) and the CO selectivity of the nano-Al_2O_3-supported catalysts can be further improved by the addition of CeO_2 or ZrO_2. Another goal is to determine if the specific ZrO_2 precursor used (nitrate or nanoparticles) and the preparation method (co-impregnation and sequential impregnation) will affect the catalytic activity and the CO_2 (or CO) selectivity. Furthermore, the CO levels in the reactor effluent will be compared to the equilibrium CO concentrations from the water–gas shift reaction to elucidate the most likely production pathway for CO (i.e. methanol decomposition or the reverse water–gas shift). As Amphlett et al. [27] stated in a related study, the equilibrium conversion in the methanol reforming reaction is well over 95% under normal reaction conditions, although conversions that high can be difficult to attain in practice. Therefore, "clearly the thermodynamics offer the incentive for developing better catalysts" [27]. The search for better catalysts is continued here using nanoparticle supports.

2. Experimental

2.1. Catalyst preparation

Catalysts in this study are named according to the concentration of the active metal oxide, promoter, and support as a mass percentage. The concentrations of CuO and ZnO are kept constant at 14–15%. These concentrations were selected after careful consideration of optimum literature values [6,17,21]. In addition to the ZnO and CuO phases, either ZrO_2 or CeO_2 were used as promoter or support and the remainder of the material is nanoparticle Al_2O_3. The catalyst labels list the species present in the catalyst and the concentration of either ZrO_2 or CeO_2, as well as the preparation method employed. For instance, the CuZnZrAl-10-CI sample consists of 15% CuO, 15% ZnO, and 10% ZrO_2 by mass, with the balance (60%) being Al_2O_3. The label CI indicates that the Cu, Zn, and Zr precursors were co-impregnated on the nanoparticle Al_2O_3 or Cu and Zn were co-impregnated on nanoparticle ZrO_2 or a mixture of nanoparticle ZrO_2 and nanoparticle Al_2O_3. All catalysts contain nanoparticle Al_2O_3 except the CuZnZr-70-NP, which is 15% CuO, 15% ZnO, and 70% nanoparticle ZrO_2 by mass. The label NP indicates when nanoparticle ZrO_2 is the zirconia precursor (as opposed to $ZrO(NO_3)_2{\cdot}6H_2O$). For the CuZnZrAl-10-NP catalyst the Cu and Zn nitrate precursors were co-impregnated on a physical mixture of ZrO_2 and Al_2O_3 nanoparticles. The label "SQ" indicates sequential impregnation, i.e. the CuO and ZnO were co-impregnated on the Al_2O_3 after deposition of the ZrO_2 precursor (see below). This information is summarized in Table 1.

All catalysts in this study were prepared via some variation of wet impregnation, either concurrently or sequentially. The catalysts CuZnZrAl-10-CI and CuZnCeAl-10-CI were prepared by dissolving (in proper amounts) $Zn(NO_3)_2{\cdot}6H_2O$ (Alfa Aesar), $Cu(NO_3)_2{\cdot}6H_2O$ (Alfa Aesar), and $ZrO(NO_3)_2{\cdot}6H_2O$ or $Ce(NO_3)_2{\cdot}6H_2O$ in 50 ml of deionized water. The nanoparticle Al_2O_3 (NanoScale, surface area ~650 m^2/g) was then dispersed in the solution, the excess

Table 1
Catalyst labels, compositions, preparation procedures and CeO_2 and ZrO_2 precursors used for the catalysts in the study.

Catalyst label[a]	Composition					Preparation	Zr or Ce precursor
	CuO (%)	ZnO (%)	ZrO_2 (%)	CeO_2 (%)	Al_2O_3 (%)		
CuZnZrAl-10-CI	15	15	10	0	60	Co-impregnation	$ZrO(NO_3)_2{\cdot}6H_2O$
CuZnCeAl-10-CI	15	15	0	10	60	Co-impregnation	$Ce(NO_3)_2{\cdot}6H_2O$
CuZnZrAl-36-CI	14	14	36	0	36	Co-impregnation	$ZrO(NO_3)_2{\cdot}6H_2O$
CuZnZrAl-10-NP	15	15	10	0	60	Co-impregnation	Nanoparticle ZrO_2
CuZnZr-70-NP	15	15	70	0	0	Co-impregnation	Nanoparticle ZrO_2
CuZnZrAl-10-SQ	15	15	10	0	60	Sequential impregnation	$ZrO(NO_3)_2{\cdot}6H_2O$

[a] Catalyst labels are based on the composition of CuO, ZnO, ZrO_2 (or CeO_2) and Al_2O_3 by weight. The CuO and ZnO concentrations are kept constant at 15% (or 14%). The concentration of ZrO_2 or CeO_2 is given in the label and the balance is Al_2O_3. The last part of the label indicates the preparation method, CI for co-impregnation, NP for co-impregnation on nanoparticle ZrO_2 and SQ for sequential impregnation.

water boiled off and the resulting paste dried at 105 °C overnight. The dried sample was calcined at 300 °C for 3 h.

The catalyst CuZnZrAl-10-NP was prepared in a similar manner except that the zirconia was added as nanoparticle ZrO_2 powder (Nanostructured and Amorphous Materials) along with the nanoparticle Al_2O_3 to the aqueous solution (50 ml) of $Zn(NO_3)_2{\cdot}6H_2O$ and $Cu(NO_3)_2{\cdot}H_2O$ (Alfa Aesar). The water was evaporated and the resultant mixture was then dried and calcined in the same manner described above.

The catalyst CuZnZr-70-NP was prepared as described above except that only ZrO_2 nanoparticles were dispersed in the aqueous solution of Cu and Zn nitrates and no Al_2O_3 was used in this catalyst formulation. After impregnation of the ZrO_2 nanopowder the resulting catalyst was dried and calcined as described above.

Finally, the sequentially precipitated CuZnZrAl-10-SQ was prepared via two sequential impregnations. First, the $ZrO(NO_3)_2{\cdot}6H_2O$ was dissolved in 50 ml water and then the Al_2O_3 nanoparticles were dispersed in the solution. The sample was then boiled down to a paste and dried overnight at 105 °C and calcined at 300 °C for 3 h. The calcined support was then ground to a fine powder. The $Zn(NO_3)_2{\cdot}6H_2O$ and $Cu(NO_3)_2{\cdot}6H_2O$ were dissolved in 50 ml water and the impregnated ZrO_2/Al_2O_3 support was dispersed in the nitrate solution. The sample was again boiled down to a paste, dried and calcined in the same manner as the other samples. All catalysts were prepared in batches of 5 grams total weight after calcination. BET, N_2O adsorption and temperature programmed reduction were performed on the calcined catalysts without further treatment.

The reference catalyst used in this study is a commercially available Süd-Chemie catalyst that is approximately 42% CuO, 47% ZnO, and 11% Al_2O_3 according to the manufacturer's specifications. This is a low temperature shift catalyst typical of what is used in the methanol reforming literature [4,28,29].

2.2. Reaction experiments

Before activity measurements the prepared catalyst powders were pressed into pellets in a 0.5″ diameter pellet die under 2 t of force exerted by a Carver press. These pellets were then crushed and particles with sizes between 500 μm and 1 mm were selected for activity testing. Catalytic activity measurements were carried out in a stainless steel reactor system which has been described in detail elsewhere [11]. Briefly, approximately 300 mg of catalyst was packed between two quartz wool plugs. The pre-mixed methanol and water solution was introduced by a KDS model 100 syringe pump. The liquids travel a very short distance to an evaporator furnace. For all catalyst experiments in this publication the water/methanol ratio was constant at 1.4 (v/v) (~3.1 mol/mol). A contact time (W/F) ratio of 0.15 kg catalyst s/mmol CH_3OH (used for experiments at constant contact time and varying temperature) corresponds to a total liquid flow rate of 0.8 ml/h and 300 mg catalyst. For experiments with varying contact times (temperature = 280 °C), the amount of catalyst in the packed bed was held constant while the inlet liquid flow rate was varied.

Argon gas at a flow rate of 15.0 sccm was used as both the carrier gas for the experiments and the internal standard for the gas chromatograph. It is important to note that because of the definition of contact time (mass of catalyst in the packed bed divided by the flow of CH_3OH in mmol/s) this carrier gas does not affect the W/F ratio. Temperature was measured by an Omega type K thermocouple at the effluent side of the packed bed. The thermocouple also helped keep the packed bed in place. The reactor was placed inside of a Barnstead Type F2100 Tube Furnace.

After exiting the reactor, the unreacted condensable species (methanol and water) are removed in an ice water condenser bath before the remaining non-condensable species enter the gas chromatograph. The chromatograph used in this study is an Agilent 6890 series online gas chromatograph equipped with both a thermal conductivity detector and a flame ionization detector in series. Since methanol is not introduced into the chromatograph, conversion is calculated by performing a carbon balance. This is justified since the only carbon containing products detected were CO and CO_2. Furthermore, it is the methanol conversion to CO and CO_2 that is of main importance in methanol reforming. All catalyst samples were activated *in situ* in 10% H_2 in Ar (45 sccm total flow rate) at 300 °C for 3 h before being exposed to the reactant mixture. This is the pretreatment recommended by the commercial catalyst manufacturer, and a very similar pretreatment has been used in related studies involving Süd-Chemie low temperature shift catalysts [5]. Since there is always a concern that the catalytic activity may be changing during the course of an experiment, or that the catalysts require extended periods of time to reach steady state [30], gas samples from the reactor effluent were collected until the compositions were stable and no longer changing, approximately 2 h after system start-up. Data points taken after significant time on stream (up to 40 h) were also repeated with fresh catalysts to determine that catalyst aging could be ruled out in the analysis. In reactor experiments when temperature was the independent variable, this corresponds to beginning the reactor experiments with a fresh load of catalyst at 300 °C to make sure the data overlaps with the experiments where the temperature sweep was started at 205 °C. Each data point is the average of five gas samples at a given temperature. This represents approximately 4 h at each temperature. The reproducibility of temperature activity curves indicates that time on stream up to ~40 h was not a factor in catalyst deactivation for the catalysts used in this study. A similar procedure was used to verify reproducibility when contact time was the independent variable. In all cases, reproducible results were obtained and there were no signs of catalyst deactivation due to aging with time on stream. Also, there was no evidence of further activation on stream. It was confirmed that performing the reaction at, for example, 280 °C before a 260 °C experiment did not give a more active catalyst compared to one that had been exposed to reaction conditions at 240 °C before the 260 °C experiment.

2.3. BET surface area analysis

Single point Brunauer–Emmett–Teller (BET) surface area measurements were performed on a Quantachrome ChemBET 3000 instrument. Samples were out-gassed under N_2 for 1 h at 100 °C. Selected results were compared to multi-point BET on a Quantachrome NOVA instrument to validate using only single point measurements.

2.4. Cu surface area measurements using N_2O titration

The copper surface area was measured on a ChemBET 3000 instrument using the N_2O decomposition method, as is typically done for copper based reforming catalysts [6,11,31]. The experimental set up has been described in detail in our earlier work [11]. In brief: the samples are first reduced in 5% H_2 in He at 300 °C (20 sccm) prior to the measurement and then cooled overnight to room temperature under helium. The total amount of N_2 formed during the N_2O decomposition over the catalysts was determined and used to calculate the amount of copper surface atoms according to the stoichiometry in Eq. (5).

$$2Cu + N_2O \rightarrow N_2 + Cu_2O \quad (5)$$

The ChemBET Instrument uses a liquid Argon cold trap to separate unreacted N_2O from N_2 formed via Eq. (5). The N_2 signal is measured using a TCD built into the instrument. In this way N_2O is titrated over the sample until no N_2 is recorded on the TCD. The total amount of N_2 formed is then found by integrating over the total N_2 signal peak areas and calibrating this against known volumes of N_2 injected into the instrument. The copper surface area was calculated from these results assuming a copper surface density of 1.47×10^{19} copper atoms per square meter [24,31]. A turnover frequency (TOF), defined as the molecules of hydrogen formed per surface copper atom per second, was calculated using the measured hydrogen production rate and copper surface area.

2.5. Temperature programmed reduction experiments

Temperature programmed reduction (TPR) measurements were also performed in the Quantachrome ChemBET 3000 instrument. For TPR measurements, 55 mg of the catalyst was loaded in a quartz tube reactor and secured with plugs of quartz wool on both ends. An Omega K-type thermocouple monitored the temperature in the catalyst bed. Reduction was carried out at a heating rate of 5 °C per minute up to a temperature of 500 °C under a flow of 5% H_2/N_2 mixture at a total flow rate of 70 sccm until the catalyst was fully reduced and did not consume additional hydrogen. The hydrogen uptake was continuously monitored using a TCD detector during the reduction.

2.6. X-ray diffraction (XRD) analysis

The XRD data was collected on a Philips powder X-ray diffractometer using Bragg-Brentano geometry with Cu Kα radiation (λ = 1.54 Å). The XRD spectra were recorded in a 2θ range of 20–80° at ambient conditions. Diffraction patterns were obtained for all samples after calcinations and again after exposure to reaction conditions. Average particle sizes were calculated from the line-broadening of the XRD peaks using the Scherrer equation [Eq. (6)].

$$d = \frac{K\lambda}{FW \cos\theta} \tag{6}$$

In this equation K is a constant generally taken as unity, λ is the wavelength of the incident radiation, FW is the full width at half maximum and θ is the peak position.

2.7. X-ray photoelectron spectroscopy analysis

Some initial XPS data was collected to confirm that ignoring carbon deposition in calculating a carbon balance is reasonable. The catalyst powders were pressed into aluminum cups prior to insertion into the ultra-high vacuum (UHV) chamber (base pressure 1×10^{-10} Torr). The XPS data was collected using a double pass cylindrical mirror analyzer (PHI model 25-270 AR) with incident radiation from a Mg Kα X-ray source (PHI 04-151). Spectra were taken in retarding mode with a pass energy of 50 eV. Data was collected and then digitally smoothed using a computer interface [32]. Charge shift corrections were made by assuming a C 1s signal of 284.6 eV [33].

2.8. Water–gas shift equilibrium

The calculated equilibrium data is presented by plotting the ratio Φ as defined in Eq. (7).

$$\Phi = \frac{P_{CO_2} P_{H_2}}{K_{WGS} P_{CO} P_{H_2O}} \tag{7}$$

This is the same procedure used in the studies of Peppley et al. [4] and Agrell et al. [5]. In this equation K_{WGS} is the temperature dependent equilibrium constant of the water–gas shift reaction, calculated from the activation energy and pre-Arrhenius factor used by Peppley et al. [34]. Since water is not measured on the gas chromatograph, the water level in the effluent gas is estimated from the CO_2 level via the reforming reaction. Specifically, since there is a 1:1 molar ratio of CO_2 produced to H_2O consumed, the moles of H_2O reacted per unit time are assumed to be equal to the (measured) moles of CO_2 produced. This number of moles of water is then subtracted from the (known) inlet molar flow rate of H_2O. The remainder is assumed to be in the effluent. The assumption used here is that the amount of water reacted in the steam reforming reaction is much greater than any water involved in the water–gas shift. This is reasonable given the disparity in the levels of CO_2 and CO in the effluent. Confidence levels are presented, and it is evident that even if the measurement is off by 20%, the conclusions are not affected. According to the definition of Φ, a value of 1 represents the water–gas shift reaction equilibrium. If $\Phi < 1$ the CO concentration is higher than what can be explained by the water–gas shift equilibrium and if $\Phi > 1$ the CO concentration is lower than the equilibrium CO water–gas shift concentration.

3. Results and discussion

3.1. Catalytic activity measurements

Fig. 1A and B show the methanol conversion as a function of temperature for all catalysts in Table 1. For comparison, the data obtained from a reference catalyst is also included in the figures. It is evident from Fig. 1A that ZrO_2 is a much better promoter of the catalysts under these conditions compared with CeO_2. The CeO_2-containing catalyst (CuZnCeAl-10-CI) never attains a conversion comparable to the commercial catalyst. In contrast, above a temperature of 280 °C the CuZnZrAl-10-CI catalyst exhibits a higher conversion than the reference catalyst. Increasing the ZrO_2 content from 10% to 36% increases the low temperature conversion, but this catalyst experiences deactivation above 265 °C. To probe how sensitive the catalysts are to preparation method and ZrO_2 precursor, two additional 10% ZrO_2 catalysts were prepared (CuZnZrAl-10-SQ and CuZnZrAl-10-NP). Consequently, the nominal chemical composition of the CuZnZrAl-10-CI, CuZnZrAl-10-SQ and CuZnZrAl-10-NP catalysts is the same. The differences are the order of Zr deposition (versus Cu and Zn) and the precursor ($ZrO(NO_3)_2{\cdot}6H_2O$ versus nanoparticle ZrO_2), as explained in Section 2. While the performances of the various CuZnZrAl-10 catalysts are similar up to 240 °C, the preparation method and the ZrO_2 precursor evidently have a large influence on the catalytic activity above this temperature. The CuZnZrAl-10-NP catalyst exhibits the best performance of all catalysts in this series, and it is the only one to achieve ~80% conversion at the reactant feed rate used in the temperature sweep experiments. This conversion is significantly higher than the maximum of 62% obtained from the commercially available reforming catalyst. Only at the lowest temperature (225 °C) does the commercial catalyst have a slightly higher conversion than the CuZnZrAl-10-NP catalyst. The CuZnZrAl-10-SQ catalyst exhibits the poorest performance of these three CuZnZrAl-10 catalysts with a maximum methanol conversion of 66%. The sequential catalyst undergoes deactivation above 285 °C in the presence of the reactant mixture, and this is the same temperature range where the reference catalyst also loses activity. In contrast, the CuZnZrAl-10-CI and the CuZnZrAl-10-NP do not deactivate until temperatures above 300 °C. A Cu-Zn catalyst supported on nanoparticle ZrO_2 was also prepared to determine if alumina is necessary to assure a high catalytic activity.

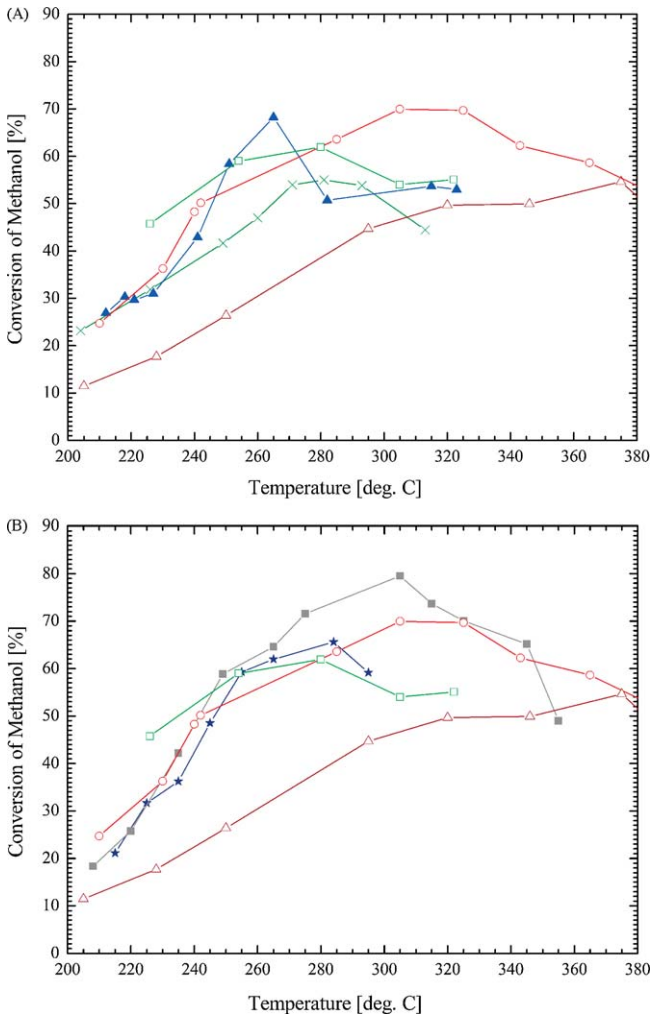

Fig. 1. (A) Methanol conversion as a function of temperature for selected catalysts. (–○–) CuZnZrAl-10-CI, (–▲–) CuZnZrAl-36-CI, (–△–) CuZnZr-70-NP, (–×–) CuZnCeAl-10-CI and (–□–) commercial reference. Contact time for all curves is 0.15 kg catalyst s/mmol CH_3OH. (B) Methanol conversion as a function of temperature for additional catalysts. (–○–) CuZnZrAl-10-CI, (–★–) CuZnZrAl-10-SQ, (–△–) CuZnZr-70-NP, (–■–) CuZnZrAl-10-NP and (–□–) commercial reference.

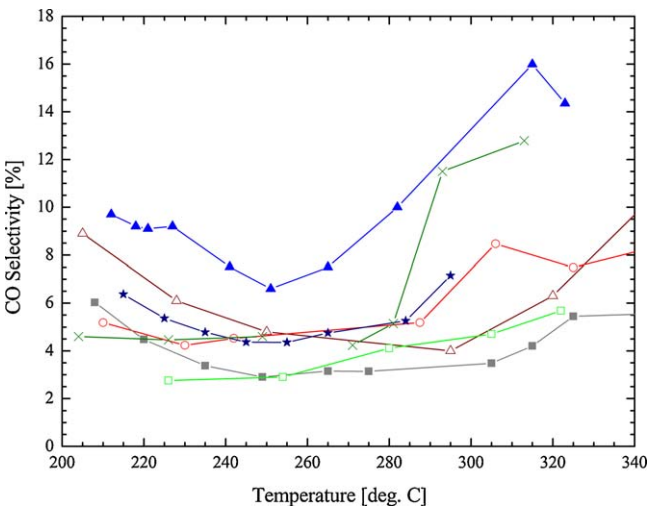

Fig. 2. CO selectivity as a function of temperature for all nanoparticle catalysts. (–○–) CuZnZrAl-10-CI, (–▲–) CuZnZrAl-36-CI, (–△–) CuZnZr-70-NP, (–×–) CuZnCeAl-10-CI, (–★–) CuZnZrAl-10-SQ, (–■–) CuZnZrAl-10-NP and (–□–) commercial reference. Contact time for all curves is 0.15 kg catalyst s/mmol CH_3OH.

The CuZnZr-70-CI catalyst exhibits the lowest maximum conversion of all catalysts in this study. Only at temperatures where the other catalysts experience significant deactivation does the CuZnZr-70-NP catalyst have a higher conversion. The temperature dependent deactivation in this study was irreversible. Reducing the catalysts a second time in 10% H_2 did not return the catalysts to the initial activity levels. We have noted a similar effect in a related study [11]. In the present case the deactivation appears to be a consequence of sintering of the Cu phase during exposure to reaction conditions (see Section 3.4) and not due to coking. However, since coking of the catalyst is important not only for catalyst deactivation, but also for closing the carbon balance, XPS survey data of fresh and spent catalysts were collected for the CuZnZrAl-10-NP, CuZnZrAl-10-CI and CuZnCeAl-10-CI catalysts. The C 1s peak area ratio for the spent/fresh catalysts was ~0.9 for all three catalysts. This indicates that there is no carbon deposition on the catalysts during the course of the reaction. Calculating the methanol conversion based on the methanol feed rate and the production rates of CO and CO_2, which were the only carbon containing products, is therefore justified.

The CO selectivity as defined in Eq. (4) is shown in Fig. 2 for all catalysts as a function of temperature. The CuZnZrAl-10-NP catalyst maintains the lowest CO selectivity of any catalyst in this study over the entire temperature range. This is remarkable considering that it also exhibits the highest conversions at these temperatures. Even at the maximum conversion (305 °C), the CuZnZrAl-10-NP catalyst exhibits a CO selectivity (3.6%) that is only slightly higher than the lowest value observed (2.9%) for this catalyst. This CO selectivity corresponds to a CO concentration of 0.6% (dry) in the reactor effluent. Of the other 10% ZrO_2 samples (CuZnZrAl-10-CI and CuZnZrAl-10-SQ), the sequentially impregnated catalyst exhibits a higher CO selectivity than the co-impregnated catalyst although the difference is not significant between 240 °C and 285 °C. The CuZnCeAl-10-CI and CuZnZrAl-10-CI catalysts exhibit similar CO selectivities below 280 °C. However, above 280 °C there is a discontinuous increase in the CO selectivity for the CuZnCeAl-10-CI catalyst that is not evident in any of the other catalysts. The steep increase in the CO selectivity for this catalyst coincides with the loss of activity as seen in Fig. 1A. Catalyst CuZnZrAl-36-CI exhibits the highest CO selectivity of the catalysts in the series. In fact, the CO selectivity of this catalyst is higher than the CO selectivities observed on the Cu-ZnO/nano-Al_2O_3 catalysts in our previous study [11]. Consequently, using an impregnation method to prepare $Cu/ZnO/ZrO_2/Al_2O_3$ catalysts it is important to use ZrO_2 concentrations below (perhaps well below) 36%. The 70% nanoparticle ZrO_2 catalyst (CuZnZr-70-NP) exhibits a lower CO selectivity than the 36% ZrO_2 sample, but it is still higher than the CO selectivity for the alumina containing samples at temperatures below 250 °C. The CO selectivity for this catalyst continues to decrease up to a temperature of 295 °C. At this temperature only the 10% nano-ZrO_2 catalyst (CuZnZrAl-10-NP) has a lower CO selectivity. The methanol conversion of the CuZnZr-70-NP catalyst is only 45% at this temperature, which indicates that this catalyst is not a competitive methanol steam reforming catalyst for PEM fuel cell applications. It is worth noting that the CO selectivity for all catalysts in this study either decreases or stays constant with increasing temperature below approximately 250 °C. This is an important observation given that the only CO production routes, the reverse water–gas shift and the methanol decomposition reaction, are both endothermic and thus CO production should be both kinetically and thermodynamically favored with increasing temperature. Consequently, the CO selectivity curves demonstrate that the methanol reforming reaction must be increasing at a faster rate than either the

decomposition reaction or the reverse water–gas shift reaction (or a combination of the two) for all catalysts. A similar phenomenon has been observed previously using (exclusively) nano-Al_2O_3-supported catalysts [11]. The temperature at which CO selectivity begins to increase is not constant for all the catalysts, but appears to be near 250 °C.

As mentioned previously, the thermodynamic equilibrium for the steam reforming reaction is over 95% methanol conversion above 200 °C with excess water present. Hence, higher conversions than those reported in Figs. 1 and 2 are possible at longer contact times. Therefore, experiments were performed on selected catalysts at constant temperature and varying contact times. Fig. 3 displays the conversion as a function of contact time for these catalysts, including the commercial reference. The temperature selected for the experiments was the temperature of maximum conversion for the commercial reference catalyst (280 °C). Only the most active catalysts with reasonably low CO conversions were subjected to the contact time activity measurements. The only exception to this is the CuZnCeAl-10-CI which was included for comparison. Again, the CuZnZrAl-10-NP catalyst exhibits the best performance of all the catalysts. The other catalysts required considerably longer contact times to reach 100% conversion. As with the conversion data shown in Fig. 1, the CeO_2-containing catalyst exhibited the lowest activity. In the absence of catalyst deactivation, such as sintering, it is expected that all catalysts in the study will achieve 100% conversion given sufficient contact time. However, as is well documented in the literature, longer contact times (i.e. higher *W*/*F* ratios) also increase the CO selectivity [2,5,7,20,29]. Therefore, it is advantageous that the CuZnZrAl-10-NP catalyst attains 100% conversion at shorter contact times than required for 100% conversion of the commercial catalyst. The shapes of the curves in Fig. 3 are also worth noting. The CuZnZrAl-10-NP and CuZnZrAl-10-CI samples both exhibit the classic shape asymptotically approaching a conversion of 100% with increasing contact times. In contrast, the CuZnZrAl-10-SQ, CuZnCeAl-10-CI and the commercial reference catalysts display a rapid increase in conversion at intermediate contact times. This behavior is generally undesirable since the rapid increase in conversion is also followed by a significant increase in the CO selectivity (see Fig. 4).

Fig. 4 displays CO selectivity as a function of contact time for the most active catalysts, as well as the CuZnCeAl-10-CI and commercial reference catalyst at 280 °C. In this figure the CO selectivity of the CuZnZrAl-10-SQ catalyst is nearly double that of the other samples at and above contact times of 0.28 kg catalyst s/mmol. Since the conversion of the CuZnZrAl-10-SQ catalyst at this contact time is only 59%, this catalyst is not suitable for methanol steam reforming reactions where low CO concentrations are critical. The most interesting feature of this figure is the CO selectivity of the CuZnZrAl-10-NP. For this sample the CO selectivity increases only slightly and then remains fairly constant with increasing contact time up to a value of 0.3 kg catalyst s/mmol. Consequently, the CuZnZrAl-10-NP catalyst is superior to the others in this study in that the conversion is increased significantly with temperature, while the CO selectivity remains almost constant.

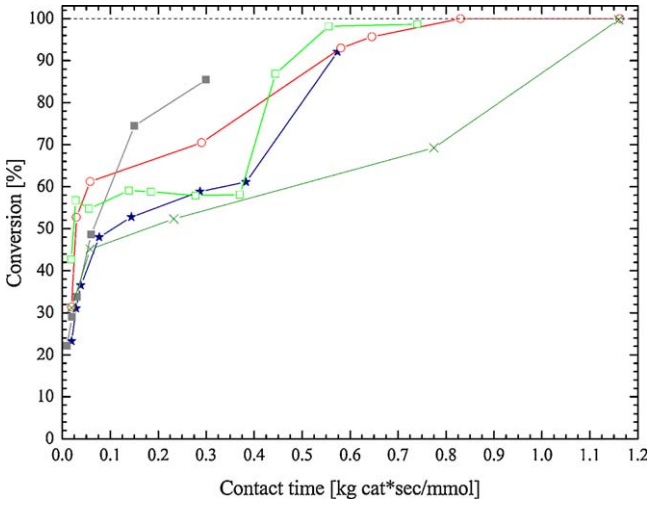

Fig. 3. Conversion as a function of contact time for the 10% ZrO_2 catalysts, the 10% CeO_2 catalyst, and the commercial reference catalyst. (—○—) CuZnZrAl-10-CI, (—★—) CuZnZrAl-10-SQ, (—■—) CuZnZrAl-10-NP, (—×—) CuZnCeAl-10-CI and (—□—) commercial reference. Temperature for all curves was held constant at 280 °C.

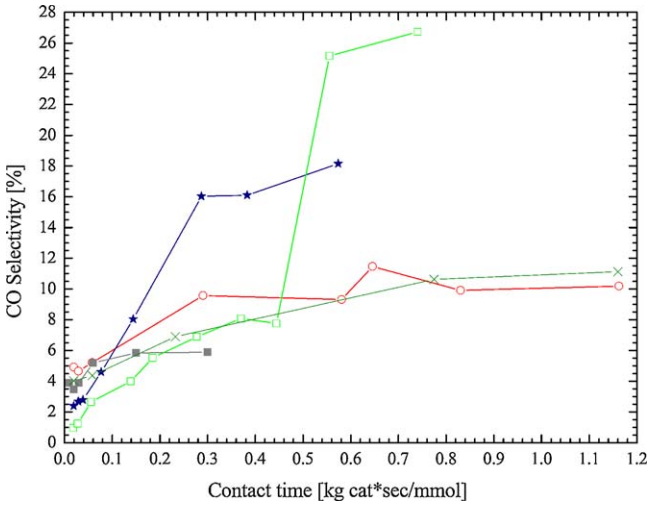

Fig. 4. CO selectivity as a function of contact time for the 10% ZrO_2 catalysts, the 10% CeO_2 catalyst, and the commercial reference catalyst. (—○—) CuZnZrAl-10-CI, (—★—) CuZnZrAl-10-SQ, (—■—) CuZnZrAl-10-NP, (—×—) CuZnCeAl-10-CI and (—□—) commercial reference. Temperature for all curves was held constant at 280 °C.

3.2. Surface area analysis

The BET surface area data, active copper surface area, copper dispersion, and turnover frequency at approximately 250 °C and 300 °C are presented in Table 2 for all catalysts. Included in the table are also results for the commercial reference catalyst and a representative catalyst from our Cu-ZnO on nanoparticle alumina series [11].

Evidently there is no correlation between the overall surface area and the Cu surface area of the catalysts, except that the catalyst with the lowest total surface area (CuZnZr-70-NP) also does have the smallest Cu surface area. As expected, the lowest Cu surface area is observed on the catalyst which does not contain any

Table 2
Surface characteristics and activities of steam reforming catalysts.

Catalyst	BET surface area (m^2)	Cu surface area (m^2/g)	Cu dispersion (%)	TOF × 10^3 (s^{-1})	
				250 °C	300 °C
CuZnZrAl-10-CI	48.0	11.3	1.7	175	226
CuZnZrAl-10-NP	115.4	11.9	1.8	220	244
CuZnZrAl-10-SQ	119.6	13.8	2.1	134	122
CuZnZrAl-36-CI	93.4	13.7	2.1	197	177
CuZnCeAl-10-CI	39.5	14.7	2.3	91	74
CuZnZr-70-NP	19.0	3.4	0.53	216	342
CuZnAl-35/35/30-CI	46	5.3	0.8	89	132
Commercial	68	20.2	3.1	34	28

high surface area nanoparticle alumina. It is, however, surprising that the different preparation methods and the varying ZrO_2 (or Al_2O_3) concentrations do not result in catalysts with a larger variation in Cu surface areas. All ZrO_2- or CeO_2-containing catalysts, except the CuZnZr-70-NP, have Cu surface areas in the range between 11 m^2/g and 15 m^2/g. Despite the similar copper surface areas the catalytic activities of the catalysts are considerably different. There is no apparent correlation between the Cu surface area and the catalytic activity on these catalysts. A very interesting observation is that the copper phase on the nanoparticle ZrO_2-supported catalysts is significantly more active than the copper on the CeO_2-promoted catalyst, the catalyst without CeO_2 or ZrO_2, as well as the catalysts prepared via impregnation using the zirconium nitrate species. This is particularly evident on the CuZnZr-70-NP catalyst, which has the lowest Cu surface area of the catalysts under investigation, but it has the highest turnover frequency observed. Consequently, the Cu on the surface of this catalyst is very active. It is also evident from Table 2 that co-impregnation of the Cu, Zn and Zr precursors results in more active catalysts than if the Zr precursor is added before the Cu and Zn precursors (sequential impregnation). It is interesting to note that the catalyst with the highest Cu surface area, the CuZnCeAl-10-CI catalyst, exhibits the lowest turnover frequency of the ZrO_2– and CeO_2–containing catalysts.

The results reveal that the nanoparticle alumina does provide a high surface area on which to deposit the active metal and promoters, which in turn is necessary to assure a reasonable Cu surface area. However, addition of ZrO_2 (or CeO_2) further improves the Cu surface area, as is evident when comparing the CuZnZrAl-10-series catalysts with the non-ZrO_2 containing CuZnAl-35/35/30-CI catalyst. Perhaps even more importantly, addition of nanoparticle ZrO_2 evidently results in a more active Cu species on the surface. This supports the notion of a "synergy" effect between the copper phase and the zirconia support, which has been documented by other researchers [6,35].

3.3. Temperature programmed reduction measurements

To further probe how the ZrO_2 influence the Cu on the surface, temperature programmed reduction experiments were performed on the prepared catalysts. The reduction profiles of all catalysts are presented in Fig. 5. The TPR data obtained from the commercial reference catalyst has also been added for comparison. It is evident that all ZrO_2- and CeO_2-containing catalysts are reduced at higher temperatures compared to the reference commercial catalyst. This is surprising, since addition of ZrO_2 and CeO_2 usually results in catalysts that are easier to reduce than their ZrO_2-free analogues [3,6,13,15]. Furthermore, the study on impregnated and precipitated CuO, ZnO, ZrO_2 and Al_2O_3 catalysts done by Breen and Ross indicated that catalysts which reduce at lower temperatures were more active methanol steam reforming catalysts [6] Evidently, the catalysts in this study do not follow this trend. In fact, the most active catalyst, CuZnZrAl-10-NP, exhibits the highest reduction temperature and a reduction profile consisting of two reduction peaks at 328 °C and 348 °C. The reduction temperatures of the CuZnZrAl-10-SQ (320 °C and 338 °C) and CuZnZrAl-10-CI (324 °C) catalysts, which are among the more active catalysts, are also higher than the other catalysts with higher ZrO_2 content. Of the ZrO_2-containing catalysts, the CuZnZr-70-NP exhibits the lowest reduction temperature (273 °C and 300 °C), which could be due to the lack of alumina. As noted previously, this catalyst also has the highest turnover frequency of any sample in this study. Accordingly, the surface of this catalyst is highly active and this agrees with the trend in reduction temperatures noted by Breen and Ross [6]. However, the sample is apparently crippled by the low Cu surface area and hence is not an effective catalyst. The CuZnZrAl-36-CI catalyst (316 °C) is only slightly more reducible than the CuZnZrAl-10-CI catalyst (324 °C) even though it has a significantly higher ZrO_2 content.

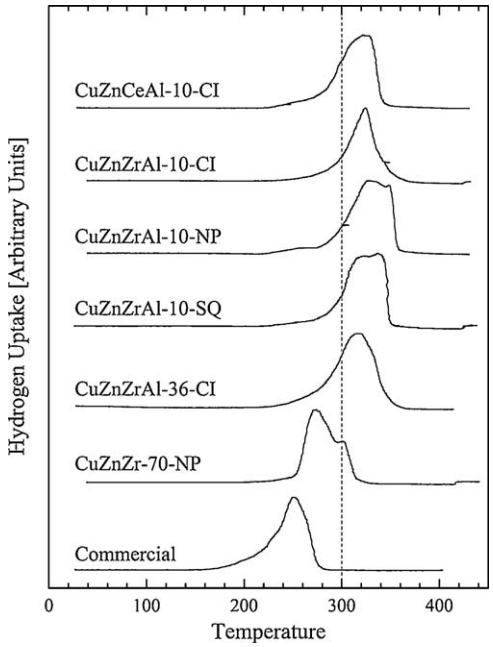

Fig. 5. Temperature programmed reduction profiles for all catalysts in this study. Curves are labeled appropriately in the figure. Dashed line has been added for visualization and shows a temperature of 300 °C. Reduction was performed under 5% H_2 in N_2 at a temperature ramp of 5 °C/min.

It is evident from Fig. 5 that the method of preparation, i.e. sequential versus co-impregnation, affects the reduction properties of the resulting catalysts. The CuZnZrAl-10-CI and CuZnZrAl-36-CI catalysts, in which the Cu, Zn and Zr precursors are impregnated onto the nano-Al_2O_3 at the same time, are the only ZrO_2-containing catalysts which exhibit a single reduction peak. All the other ZrO_2-containing catalysts exhibit two distinct reduction peaks. While it is possible that the two reduction peaks are due to a step-wise reduction of CuO via Cu_2O to Cu metal [12], another explanation is that the two peaks are due to different types of Cu on the surface [15]. These two copper species could be a highly dispersed copper phase together with larger copper particles [6,13]. In addition, copper supported on monoclinic ZrO_2 has been shown to give two reduction peaks due to copper interactions with two different types of oxygen on the ZrO_2 surface [36]. It is not easy to explain why the CuZnZrAl-10-NP and CuZnZrAl-10-SQ catalysts would result in a two-step reduction of CuO, while the CuO on the CuZnZrAl-10-CI catalyst would reduce to Cu metal in one step. Therefore, it may be more likely that the two reduction peaks are due to the presence of two different Cu species on the surface. The ZrO_2 nanoparticles consist of mainly the monoclinic phase (see Section 3.4 below). If this phase indeed results in two different copper–oxygen interactions at the surface, then it is expected that the two reduction peaks would be more distinct on the CuZnZr-70-NP compared with the CuZnZrAl-10-NP catalyst, which is observed. However, this does not rule out the presence of widely varying Cu particle sizes on the surface, i.e. highly dispersed Cu and larger Cu particles. Evidently, the copper phases on the CuZnZrAl-10-SQ and CuZnZrAl-10-NP catalysts exhibit similar reduction behavior, since they both display two distinct reduction peaks. The same is true for the CuZnZrAl-36-CI catalyst, although this catalyst has a shoulder at higher temperature which is probably due to the higher ZrO_2 content.

Of the catalysts with a 10% reducible oxide concentration, the CuZnCeAl-10-CI exhibits the lowest reduction temperature

(326 °C, with a shoulder at 308 °C) and reduction is complete at a lower temperature than any of the 10–36% ZrO_2-containing catalysts. Despite the lower reduction temperature and the higher Cu surface area, the CuZnCeAl-10-CI has a lower catalytic activity than any of the ZrO_2-containing catalysts. Therefore, under these conditions there is no correlation between the methanol conversion or turnover frequency and the reduction temperature of the catalyst for this series of catalysts. In agreement with our results there are recent studies which indicate that the reducibility of the copper species does not play the decisive role in determining catalytic performance, and in some cases the catalysts which are more difficult to reduce tend to be more active [35,37].

3.4. X-ray diffraction analysis

Fig. 6A shows the XRD spectra collected from all catalysts after calcination. The characteristic peaks of CuO are evident on all samples, as expected. None of the impregnated zirconia samples exhibit a crystalline ZrO_2 phase. The monoclinic ZrO_2 phase of the nanoparticle zirconia is evident on catalysts where the ZrO_2 nanoparticles are used in the catalyst preparation (NP catalysts). It is interesting that even for the case of the CuZnZrAl-36-CI sample no crystalline ZrO_2 phase is present. In fact, the catalyst with 36% ZrO_2 exhibits the poorest crystallinity of the catalysts in this

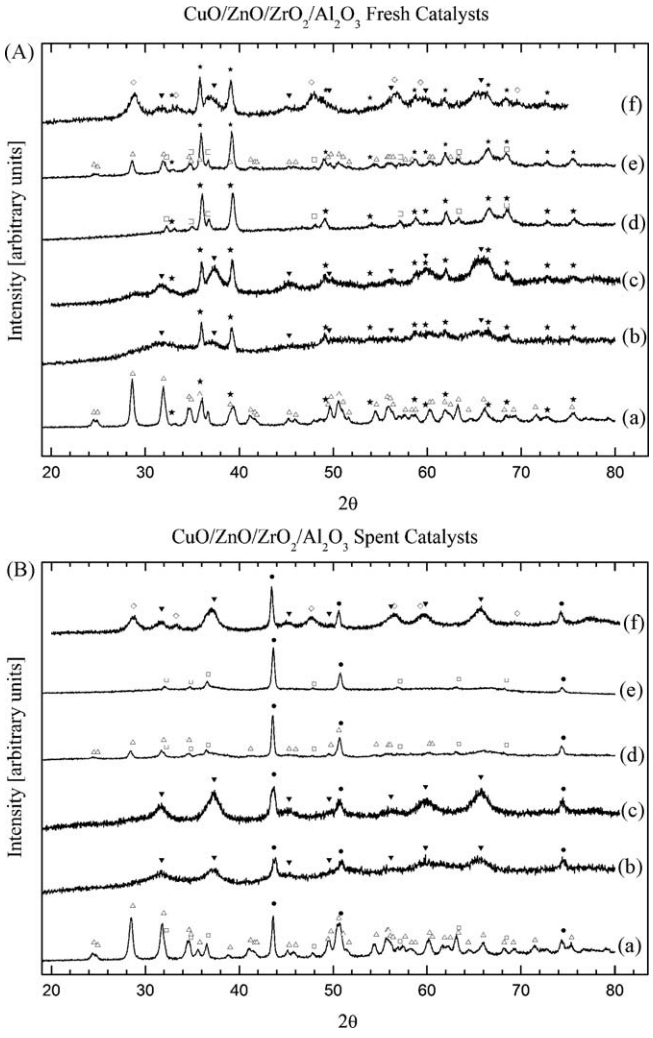

Fig. 6. XRD spectra obtained for all (A) fresh and (B) spent catalysts. (a) CuZnZr-70-NP, (b) CuZnZrAl-36-CI, (c) CuZnZrAl-10-CI, (d) CuZnZrAl-10-NP, (e) CuZnZrAl-10-SQ and (f) CuZnCeAl-10-CI. (◇) Cubic CeO_2, (▼) $ZnAl_2O_4$, (★) CuO, (●) Cu, (□) ZnO and (△) monoclinic ZrO_2.

Table 3
Particle sizes of the different compounds on the various $CuO/ZnO/ZrO_2/Al_2O_3$ catalysts in the current work. The particle sizes have been determined from the XRD data using the Scherrer equation.

Particle sizes (nm)						
Catalyst	Species					
	Cu	CuO	ZnO	$ZnAl_2O_4$	ZrO_2	CeO_2
CuZnZrAl-10-CI fresh	–	21.2	–	5.4	–	–
CuZnZrAl-10-CI spent	15.5	–	–	6.0	–	–
CuZnZrAl-10-SQ fresh	–	20.0	25.8	–	–	–
CuZnZrAl-10-SQ spent	30.0	–	28.0	–	–	–
CuZnZrAl-10-NP fresh	–	22.2	21.3	–	20.0	–
CuZnZrAl-10-NP spent	36.4	–	38.9	–	20.3	–
CuZnZr-70-NP fresh	–	13.1	–	–	19.1	–
CuZnZr-70-NP spent	30.6	–	–	–	19.0	–
CuZnZrAl-36-CI fresh	–	21.6		6.8	–	–
CuZnZrAl-36-CI spent	13.5	–		5.2	–	–
CuZnCeAl-10-CI fresh	–	17.0	–	5.8	–	6.3
CuZnCeAl-10-CI spent	30.5	–	–	5.9	–	7.4

investigation, with only the CuO phase and a poorly crystalline $ZnAl_2O_4$ spinel phase evident from the spectra. The CuZnZr-70-NP sample is highly crystalline with all three phases (CuO, ZnO, ZrO_2) evident in the XRD spectra. There is a spinel $ZnAl_2O_4$ phase present on the CuZnZrAl-10-CI and CuZnCeAl-10-CI, and CuZnZrAl-36-CI catalysts. We have documented this spinel phase in our previous work [11]. This phase does not form during the sequential preparation method, when the ZrO_2 is deposited first, and it also appears to be hindered by the presence of the nanoparticle ZrO_2. Particle size information presented in Table 3 was calculated using the (1 1 1) peak position and the full width at half maximum of CuO, ZrO_2, CeO_2 (when present) and $ZnAl_2O_4$. Fig. 6B shows the spectra from the spent catalysts after the temperature sweep experiments shown in Fig. 1. The large well defined peak at 43° is the (1 1 1) peak of Cu metal which is evident in all samples. This peak was used to calculate the Cu metal particle size of the spent catalysts. The CeO_2, ZrO_2 and $ZnAl_2O_4$ phases are not significantly altered by exposure to reaction conditions (see Table 3). In contrast, there is a significant increase in the Cu particle size after exposure to reaction conditions for all catalysts except the CuZnZrAl-10-CI and CuZnZrAl-36-CI, compared to the particle size of the original CuO after calcination. This increase in Cu particle size is evidence of significant sintering of the catalysts. This is the most likely explanation for the deactivation evident in Fig. 1.

3.5. Equilibrium calculations

Fig. 7 shows the Φ ratio, as defined in Eq. (7), for selected catalysts as a function of temperature. This analysis takes into account that the K_{WGS} value changes as a function of temperature. The same approach was originally performed by Graaf et al. in their investigation of the water–gas shift equilibria [38]. As can be seen in the figure, $\Phi < 1$ at all temperatures for both the CuZnZrAl-36-CI and CuZnZrAl-10-SQ catalysts, which means that the CO concentrations in the reactor effluent are higher than the water–gas shift equilibrium CO concentration. These two catalysts were representative of all prepared catalysts except the CuZnZrAl-10-NP. Only the CuZnZrAl-10-NP catalyst gives values of $\Phi > 1.0$. This indicates that CO is present at levels below the WGS equilibrium concentration for the CuZnZrAl-10-NP catalyst at temperatures between 300 °C and 325 °C. For all the other catalysts the CO concentration is higher than what can be explained by the water–gas shift equilibrium concentration, indicating that the source of CO must be from another reaction, i.e. the methanol decomposition reaction. This is in agreement with the observation by Peppley et al. [4]. The CuZnZrAl-10-NP catalyst appears to suppress the

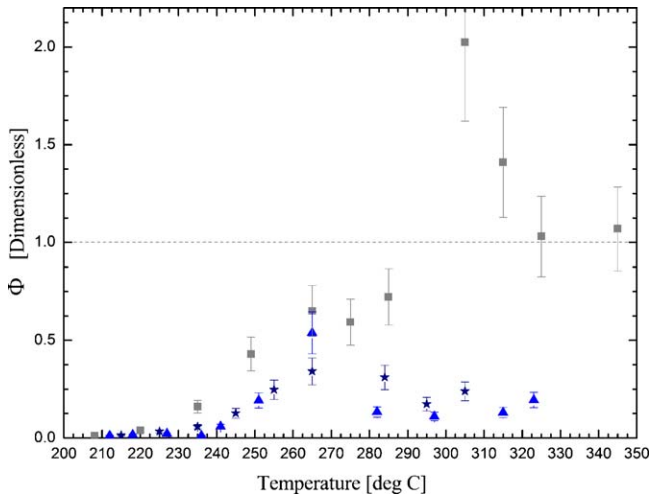

Fig. 7. Dimensionless water–gas shift equilibrium constant, Φ, as a function of temperature three nanoparticle catalysts. (▲) CuZnZrAl-36-CI, (★) CuZnZrAl-10-SQ and (■) CuZnZrAl-10-NP. Contact time for all curves is 0.15 kg catalyst s/mmol CH_3OH which corresponds to 300 mg catalyst and a total liquid inlet flow rate of 0.8 ml/h. Dashed line corresponds to the equilibrium value ($\Phi = 1$).

decomposition reaction and the system approaches the water–gas shift equilibrium at temperatures above 300 °C. The fact that it is possible to achieve CO concentrations in the reactor effluent below that of the water–gas shift equilibrium at methanol conversions of 80% for the CuZnZrAl-10-NP catalyst reveals that this is a very promising methanol steam reforming catalyst for PEM fuel cell applications.

Evidently, presence of nanoparticle ZrO_2 results in a highly active catalyst surface. The difference in performance of the nanoparticle ZrO_2 catalyst versus the two impregnated samples is likely a consequence of differences in the nature of the zirconia phase. It has been shown by Bell that in the methanol synthesis reaction the system is highly sensitive to the zirconia phase [39,40]. For instance, methanol synthesis catalysts supported on monoclinic ZrO_2 are more active than those supported on tetragonal ZrO_2 [39,40]. It has further been demonstrated that during calcination of impregnated zirconia catalysts, the ZrO_2 first forms as an amorphous phase, and then the metastable tetragonal phase forms below 550 °C [41,42]. Monoclinic ZrO_2 forms only above 550 °C, which is much higher than the calcinations used in this work. In our case, however, the ZrO_2 nanoparticles consist of mainly a monoclinic ZrO_2 phase. Therefore, the CuZnZrAl-10-NP and the CuZnZr-70-NP catalysts, which exhibit the highest turnover frequencies in this study, are also the only two catalysts that contain a monoclinic ZrO_2 phase, as seen in the XRD spectra. The fact that the ZrO_2-containing catalysts appear to suppress CO formation could be due to a stabilization of a Cu^+ species on the surface [15,18,19]. This is supported by the observation that CO is adsorbed more strongly on Cu_2O compared with Cu metal [43], which means that CO desorption would not be as facile on a Cu_2O covered surface. Furthermore, there would also be oxygen present for oxidation of the CO to CO_2, which is important since the CO production has been shown to increase with increasing extent of reduction of the catalyst [44].

4. Conclusions

Addition of ZrO_2 to Cu-ZnO catalysts supported on nanoparticle alumina results in highly active methanol reforming catalysts. Under similar conditions, our ZrO_2-promoted catalysts achieve higher methanol conversions and lower CO selectivities in the methanol steam reforming reaction compared to the commercial reference catalyst. The catalysts are sensitive to both preparation method and ZrO_2 precursor. The best performing catalyst is the CuZnZrAl-10-NP, in which the ZrO_2 is added in the form of nanoparticles. Only the CuZnZr-70-NP catalyst exhibits a higher turnover frequency than the CuZnZrAl-10-NP catalyst. However, since the CuZnZr-70-NP catalyst does not contain any high surface area alumina, this catalyst is limited by its low Cu surface area.

There is no simple correlation between the Cu surface area and the catalytic activity (methanol conversion and turnover frequency) for the ZrO_2- and CeO_2-promoted catalysts in this study. It is instead necessary to consider the catalyst preparation method and the influence of the precursor materials to determine which catalyst is superior. Under the conditions used in the study, CeO_2 is a much less efficient promoter compared with ZrO_2. It is evident from the high turn over frequencies of the CuZnZr-70-NP and CuZnZrAl-10-NP that the use of nanoparticle ZrO_2 results in a very active Cu phase on the surface, possibly due to the monoclinic ZrO_2 phase. Furthermore, there is no correlation between the reduction temperature and the catalytic activity under the conditions used. In contrast to most literature data, in the present study the best performing catalyst exhibits the highest reduction temperature.

Another interesting result is that the CO selectivities over our nanoparticle-supported catalysts decrease with temperature below 250–300 °C. This indicates that the steam reforming reaction rate (Eq. (1)) increases faster than the reverse water–gas shift (Eq. (2)) and the methanol decomposition (Eq. (3)) reaction rates with increasing temperature. Despite this, the CO levels for most of our catalysts are above the water–gas shift equilibrium concentration, which indicate that the CO decomposition reaction must be considered.

Acknowledgements

This work was supported by NASA Glenn Research Center, Grant NAG 3-2930, monitored by Mr. Tim Smith. The authors would also like to thank Oseas Ayerdi for help with catalyst preparations and data processing of the GC measurements.

References

[1] J. Leddy, J. Fenton, Electrochem. Soc. Interface 14 (3) (2005) 21–23.
[2] A. Mastalir, B. Frank, A. Szizybalski, H. Soerijanto, A. Deshpande, M. Niederberger, R. Schomacker, R. Schlogl, T. Ressler, J. Catal. 230 (2005) 464–475.
[3] I. Ritzkopf, S. Vukojević, C. Weidenthaler, JD. Grunwaldt, F. Smith, Appl. Catal., A 302 (2006) 215–223.
[4] B. Peppley, J.C. Amphlett, L.M. Kearns, R.F. Mann, Appl. Catal., A 179 (1999) 21–29.
[5] J. Agrell, H. Birgersson, M. Boutonnet, J. Power Sources 106 (2002) 249–257.
[6] J.P. Breen, J.R.H. Ross, Catal. Today 51 (1999) 521–533.
[7] J.P. Breen, F.C. Meunier, J.R.H. Ross, Chem. Commun. (1999) 2247–2248.
[8] N.E. Vanderborgh, B.E. Goodby, T.E. Springer, Proc. 32nd Int. Power Sources Symp., 1986, 623–628.
[9] R. Figueiredo, A. Martinez-Arias, M. Granados, J.L. Fierro, J. Catal. 178 (1998) 146–152.
[10] P.H. Matter, D.J. Braden, U.S. Ozkan, J. Catal. 223 (2004) 340–351.
[11] S.D. Jones, L.M. Neal, H.E. Hagelin-Weaver, Appl. Catal., B 84 (2008) 631–642.
[12] B. Lindström, L.J. Pettersson, P.G. Menon, Appl. Catal., A 234 (2002) 111–125.
[13] H. Jeong, K. Kim, T. Kim, C. Ko, H. Park, I. Song, J. Power Sources 159 (2006) 1296–1299.
[14] X.R. Zhang, P. Shi, J. Zhao, M. Zhao, C. Liu, Fuel Proc. Technol. 83 (2003) 183–192.
[15] J. Agrell, H. Birgersson, M. Boutonnet, I. Melián-Cabrera, R.M. Navarro, J.L.G. Fierro, J. Catal. 219 (2003) 389–403.
[16] L. Yong-Feng, D. Xin-Fa, L. Wei-Ming, Int. J. Hydrogen Energy 29 (2004) 1617–1621.
[17] W.-H. Cheng, I. Chen, J.-S. Liou, S.-S. Lin, Topics Catal. 22 (2003) 225–233.
[18] H. Oguchi, T. Nishiguchi, T. Matsumoto, H. Kanai, K. Utani, Y. Matsumura, S. Imamura, Appl. Catal., A 281 (2005) 69–73.
[19] H. Oguchi, H. Kanai, K. Utani, Y. Matsumura, S. Imamura, Appl. Catal., A 293 (2005) 64–70.
[20] H. Purnama, F. Girgsdies, T. Ressler, J.H. Schattka, R.A. Caruso, R. Schomacker, R. Schogl, Catal. Lett. 94 (2004) 61–68.
[21] Y. Men, H. Gnaser, R. Zapf, V. Hessel, C. Ziegler, Catal. Commun. 5 (2004) 671–675.
[22] Y. Men, H. Gnaser, C. Ziegler, R. Zapf, V. Hessel, G. Kolb, Catal. Lett. 105 (2005) 35–40.

[23] L.-C. Wang, Q. Liu, M. Chen, Y.-M. Liu, Y. Cao, H.-Y. He, K.-N. Fan, J. Phys. Chem. C 111 (2007) 16549–16557.
[24] A. Szizybalski, F. Girgsdies, A. Rabis, Y. Wang, M. Niederberger, T. Ressler, J. Catal. 233 (2005) 297–307.
[25] Y. Liu, T. Hayakawa, K. Suzuki, S. Hamakawa, Catal. Commun. 2 (2001) 195–200.
[26] X. Zhang, P. Shi, J. Mol. Catal. A 194 (2003) 99–105.
[27] J.C. Amphlett, M.J. Evans, R.A. Jones, R.F. Mann, R.D. Weir, Can. J. Chem. Eng. 59 (1981) 720–726.
[28] Y. Choi, H. Stenger, Appl. Catal., B 38 (2002) 259–269.
[29] H. Purnama, T. Ressler, R.E. Jentoft, H. Soerijanto, R. Schlogl, R. Schomacker, Appl. Catal., A 259 (2004) 83–94.
[30] T. Valdés-Solís, G. Marbán, A.B. Fuertes, Catal. Today 116 (2006) 354–360.
[31] G.C. Chinchen, C.M. Hay, H.D. Vandervell, K.C. Waugh, J. Catal. 103 (1987) 79–86.
[32] H.A.E. Hagelin, J.F. Weaver, G.B. Hoflund, G.N. Salaita, J. Electron Spectrosc. Relat. Phenom. 124 (2002) 1–14.
[33] C.D. Wagner, W.M. Riggs, L.E. Davis, J.F. Moulder, G.E. Muilenberg (Eds.), Handbook of X-ray Photoelectron Spectroscopy, PerkinElmer Corporation, Eden Prairie, MN, 1978.
[34] B.A. Peppley, J.C. Amphlett, L.M. Kearns, R.F. Mann, Appl. Catal., A 179 (1999) 31–49.
[35] C.Z. Yao, L.C. Wang, Y.M. Liu, G.S. Wu, Y. Cao, W.L. Dai, H.Y. He, K.N. Fan, Appl. Catal., A 297 (2006) 151–158.
[36] Y. Zhao, K. Tao, H.L. Wan, Catal. Commun. 5 (2004) 249–252.
[37] M.M. Günter, T. Ressler, R.E. Jentoft, B. Bems, J. Catal. 203 (2001) 133–149.
[38] G.H. Graaf, P.J.J.M. Sijtsema, E.J. Stamhuis, G.E.H. Joosten, Chem. Eng. Sci. 41 (1986) 2883–2890.
[39] K.T. Jung, A.T. Bell, Catal. Lett. 80 (2002) 63–68.
[40] M.D. Rhodes, A.T. Bell, J. Catal. 233 (2005) 198–209.
[41] L.C. Wang, Q. Liu, M. Chen, Y.M. Liu, Y. Cao, H.Y. He, K.N. Fan, J. Phys. Chem. C 111 (2007) 16549–16557.
[42] G. Wu, Y. Sun, Y.W. Li, H. Jiao, H.W. Xiang, Y. Xu, J. Mol. Struct. 626 (2003) 287–293.
[43] M. Turco, G. Bagnasco, U. Costantino, F. Marmottini, T. Montanari, G. Ramis, G. Busca, J. Catal. 228 (2004) 56–65.
[44] P. Pfeifer, K. Schubert, G. Emig, Appl. Catal., A 286 (2005) 175–185.